

Spectrometric Characterization for Triple-Junction Solar Cells

Johanna Aulich,* David Chojniak,* Alexander J. Bett,* Marc Steiner, Florian Schindler, Gerald Siefer, Martin C. Schubert, Jan Christoph Goldschmidt, and Stefan W. Glunz

Spectrometric characterization allows for accurate determination of the current matching point and investigation of sub-cell properties of multi-junction solar cells. It is widely used for dual-junction solar cells. Although the concept is suggested for triple-junction solar cells, it is only applied for the variation of two sub-cells. In this work, the applicability and evaluation procedure for a systematic variation of all three sub-cells of a triple-junction solar cell are presented. Clearly defined measurement conditions are derived which allow for meaningful characterization and comparisons of different triple-junction devices. The presented procedure is exemplarily tested on a III–V on silicon triple-junction solar cell using an light-emitting diode-based solar simulator where all needed spectral conditions can be calculated in advance and accordingly adjusted. Spectral conditions around the air mass 1.5 global spectrum are chosen and a fit routine to determine the current matching point from the discrete measurement points is proposed and validated by a measurement with a higher resolution around the current matching point. Finally, it is shown that the spectral conditions applied during the measurement also reflect outdoor conditions. This highlights the relevance of the presented procedure beyond the determination of the current-matching conditions.

1. Introduction

Silicon single-junction solar cells are approaching their efficiency limit of 29.4% (under the air mass 1.5 global [AM 1.5 g] spectrum at 25 °C).^[1] An approach to overcome this limit is adding additional sub-cells to the silicon single-junction solar cell to reduce thermalization losses. Perovskite on silicon dual-junction solar cells are extensively investigated in recent years, resulting in a current record efficiency of 33.7%.^[2] By including additional sub-cells, thermalization losses can be reduced further resulting in an even higher power conversion efficiency potential.^[3] Perovskite/perovskite/silicon triple-junction solar cells are not yet at such a high-efficiency level, but are gaining in importance in the research community.^[4–7] With a wafer-bonded III–V on silicon triple-junction solar cell, an efficiency of 35.9% was already achieved.^[8]

For the optimization of monolithic multi-junction solar cells, it is important to know which of the sub-cells is limiting the overall current of the device under spectral conditions of interest. Integrating the measured external quantum efficiency (EQE) should be avoided for that purpose. Measuring an absolute EQE is generally challenging,^[9] especially for multi-junction solar cells. The sub-cell to be measured has to operate in short-circuit conditions. As the single-sub-cell voltages cannot be determined individually, the operational point might differ from the actual short-circuit current condition. This can lead to a wrong absolute value of the EQE and measurement artifacts if the sub-cell to be measured suffers from a low parallel resistance.^[10] Similar effects can originate from luminescent coupling which is discussed in detail by Steiner et al.^[11] When perovskite sub-cells are involved, it becomes even more complicated. Due to dynamic effects, the EQE of perovskite solar cells can additionally depend on measurement conditions, such as bias illumination intensity or chopper frequency.^[12–15] The challenges of measuring EQE for perovskite-based dual-junction solar cells are described by Song et al.^[16]

A more accurate method to determine the current matching situation in a multi-junction device is spectrometric characterization. This method was first used on amorphous silicon dual-junction solar cells by Adelhelm and Bücher and later described in detail for III–V dual-junction solar cells by Meusel et al.^[17,18]

J. Aulich, D. Chojniak, A. J. Bett, M. Steiner, F. Schindler, G. Siefer, M. C. Schubert, S. W. Glunz
Fraunhofer Institute for Solar Energy Systems ISE
Heidenhofstrasse 2, 79110 Freiburg, Germany
E-mail: johanna.aulich@ise.fraunhofer.de;
david.chojniak@ise.fraunhofer.de; alexander.bett@ise.fraunhofer.de

J. C. Goldschmidt
Department of Physics
Group Solar Energy Conversion
Phillips-Universität Marburg
Renthof 7, 35032 Marburg, Germany

S. W. Glunz
Department of Sustainable Systems Engineering INATECH
University of Freiburg
Emmy-Noether-Strasse 2, 79110 Freiburg, Germany

 The ORCID identification number(s) for the author(s) of this article can be found under <https://doi.org/10.1002/solr.202300783>.

© 2023 The Authors. Solar RRL published by Wiley-VCH GmbH. This is an open access article under the terms of the Creative Commons Attribution License, which permits use, distribution and reproduction in any medium, provided the original work is properly cited.

DOI: 10.1002/solr.202300783

The concept is to measure current–voltage (*IV*) curves under different spectral conditions. The conditions are varied from redshifted spectra (related to a reference spectrum) where the top solar cell limits the overall current to blueshifted spectra where the bottom solar cell is limiting the current of the dual-junction device. Within this systematic approach, each spectral condition is well defined. Spectra are chosen such that the sum of the effective irradiances on all sub-cells always stays constant. This means that the photocurrent ratios (photocurrent under actual spectrum divided by photocurrent under reference spectrum) of all sub-cells are kept constant (i.e., if the top-cell photocurrent is increased the bottom-cell photocurrent is decreased and vice versa).^[18] This method not only allows for determination of the current matching point but also to investigate different effects of the individual sub-cells on the tandem *IV* curve. Additionally, by keeping the effective irradiance on the device constant, the performance potential of a certain solar cell architecture with all sub-cells optimized for standard testing conditions can be estimated.^[18] Spectrometric characterization has been widely used for III–V multi-junction solar cells,^[18–21] and meanwhile also for perovskite/silicon dual-junction solar cells.^[22–25] However, the application of this method for triple-junction solar cells is challenging as the current ratios of three sub-cells must be varied leading to a significantly higher number of spectral conditions for which *IV* measurements need to be conducted. In addition to a long measurement time, it is also time-consuming to adjust a solar simulator to all these different conditions. So far, in case of triple-junction solar cells, spectrometric characterization has only been performed between two sub-cells, holding the current of the third one constant.^[19,20] The variation of one sub-cell while the others are kept constant has also been conducted to observe effects of luminescence coupling.^[11] A complete spectrometric characterization for a triple-junction device has not been conducted yet.

In this work, we apply the method of spectrometric characterization suggested by Meusel et al.^[18] to triple-junction solar cells by conducting a full measurement with systematic spectral variations in all three sub-cells. We first introduce the methodology and theoretically discuss different current-matching scenarios. Afterward, we conduct a full spectrometric characterization on a two terminal wafer-bonded gallium indium phosphide/gallium arsenide//silicon (GaInP/GaAs//Si) triple-junction solar cell^[26] using an light-emitting diode (LED)-based solar simulator.^[27] The different spectral conditions can be calculated in advance according to the procedure described in our previous work.^[28] Based on these previously determined simulator settings, the complete spectrometric characterization is measured automatically using an in-house software to control the solar simulator spectrum. Finally, we discuss the relevance of the spectra used for real outdoor conditions.

2. Method of Spectrometric Characterization for Triple-Junction Solar Cells

In this section, we show how the principle of spectrometric characterization for dual-junction solar cells described in detail by Meusel et al.^[18] can be extended for triple-junction devices. In the dual-junction case, each spectral condition is clearly defined by a parameter *z* according to^[18]

$$j_{\text{top}}^{\text{sim}} = (1 + z)j_{\text{top}}^{\text{ref}} \quad (1)$$

$$j_{\text{bot}}^{\text{sim}} = (1 - z)j_{\text{bot}}^{\text{ref}} \quad (2)$$

where j^{sim} and j^{ref} denote the photocurrent density under the simulator and the reference spectrum, for example the AM 1.5 g spectrum, respectively, for the top and bottom solar cell. For $z > 0$ the top-cell current is increased, and the bottom-cell current is decreased compared to the reference spectrum, i.e., the spectrum is blueshifted. For $z < 0$, it is the opposite case, the spectrum is redshifted. Reference spectral conditions are applied if $z = 0$ and therefore $1 + z = 1 - z = 1$. To keep the effective irradiance on the overall device constant, the sum of the sub-cell current ratios remains fixed and equal to 2 for all spectral conditions.^[18]

$$\frac{j_{\text{top}}^{\text{sim}}}{j_{\text{top}}^{\text{ref}}} + \frac{j_{\text{bot}}^{\text{sim}}}{j_{\text{bot}}^{\text{ref}}} = (1 + z) + (1 - z) = 2 \quad (3)$$

Therefore, all spectra used for the spectrometric characterization can be described as laying on a line in the spectrometric plane.^[18]

In the case of a triple-junction solar cell, we define three parameters *A*, *B*, and *C* referred to as metric parameters in the following:

$$j_{\text{top}}^{\text{sim}} = A j_{\text{top}}^{\text{ref}} \quad (4)$$

$$j_{\text{mid}}^{\text{sim}} = B j_{\text{mid}}^{\text{ref}} \quad (5)$$

$$j_{\text{bot}}^{\text{sim}} = C j_{\text{bot}}^{\text{ref}} \quad (6)$$

The parameter *A* is used to vary the photocurrent generated in the top cell, parameter *B* the current generated in the middle cell and parameter *C* the one of the bottom cell. The reference condition corresponds to the parameter set $A = B = C = 1$. Following the principle of the dual-junction metric, we require that the sum of the photocurrent ratios is constant for all spectral conditions and equal to 3 in the triple-junction case:

$$\frac{j_{\text{top}}^{\text{sim}}}{j_{\text{top}}^{\text{ref}}} + \frac{j_{\text{mid}}^{\text{sim}}}{j_{\text{mid}}^{\text{ref}}} + \frac{j_{\text{bot}}^{\text{sim}}}{j_{\text{bot}}^{\text{ref}}} = A + B + C = 3 \quad (7)$$

Thus, the three metric parameters are not independent from each other. Allowing only physically meaningful values ($A, B, C > 0$), Equation (7) defines the plane of measurement represented in **Figure 1a**. All possible spectra which can be used for the spectrometric characterization are located in this plane.

To improve readability, it is possible to reduce the dimensionality of the plane of measurement by projecting the axis of one metric parameter onto the plane of the remaining two parameters. In this work, we project the *C* axis onto the *A*–*B* plane, resulting in a 2D triangular plane with $C = 3$ at the origin and $C = 0$ along the $B = 3 - A$ line (Figure 1b). *C* is constant on all lines which are parallel to the $B = 3 - A$ line with increasing values toward the origin. In this work, the projection of *C* is chosen, which means that the top- and middle-cell variations can directly be seen on the *x* and *y* axis, respectively. We use this representation as we are investigating silicon-based triple-

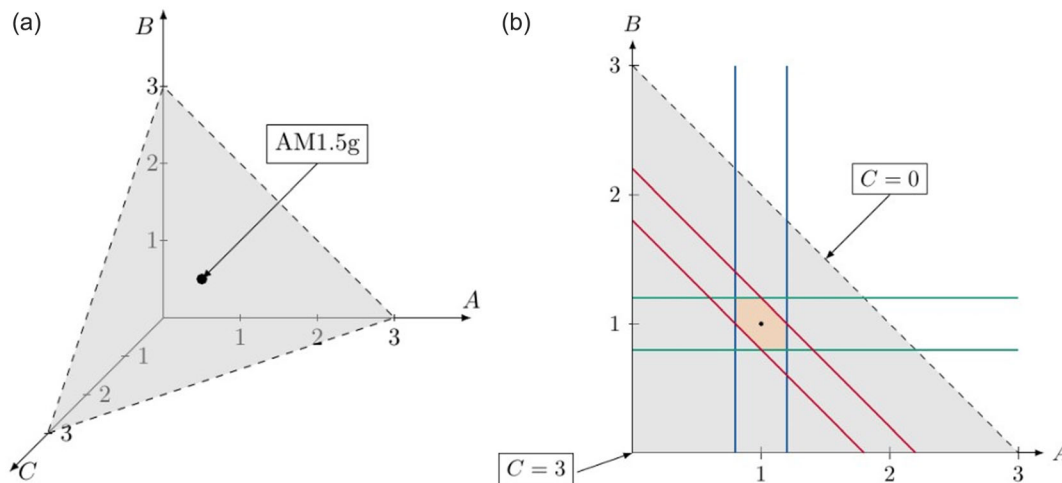


Figure 1. a) Plane of measurement defined by the boundary conditions $A, B, C > 0$ and $A + B + C = 3$. b) Plane of measurement projected on the A - B plane. C is constant for lines parallel to the $B = 3 - A$ line. Restricting A (blue vertical lines), B (green horizontal lines), and C (red diagonal lines) to $x_{\min} = 0.8$ and $x_{\max} = 1.2$ leads to the highlighted hexagonal measurement area.

junction solar cells where the bandgap of the bottom cell is fixed. However, projecting the A axis on the B - C plane or the B axis on the A - C plane would not change any result.

A spectrometric measurement is typically restricted to a certain subset of $[A, B, C(A, B)]$ around the reference spectrum. Measuring the whole plane might be not feasible due to time reasons on the one hand and limitations of the solar simulator's spectral settings on the other hand. To investigate the entire measurement plane, the irradiance on one sub-cell, i.e., one part of the spectrum, would have to be increased by a factor of three compared to the standard one sun setting. Thus, all metric parameters are restricted to a range from x_{\min} to x_{\max} , which results in a hexagonal measurement area within the plane of measurement. In Figure 1b, this is exemplarily shown for $x_{\min} = 0.8$ and $x_{\max} = 1.2$ (the photocurrents of all sub-cells are increased and decreased by 20% compared to the reference spectrum).

3. Theoretical Investigation of Different Current-Matching Scenarios

To gain a better understanding of the results that can be expected from a spectrometric measurement of a triple-junction solar cell, different current-matching scenarios are investigated using assumed current values for the three sub-cells under the reference spectrum. Based on these values, the short-circuit current density (J_{SC}) of the triple-junction solar cell is calculated by $J_{SC} = \min(j_{\text{top}}, j_{\text{top}}, j_{\text{top}})$ for each metric parameter set (A, B, C) within the measurement area defined by $x_{\min} = 0.8$ and $x_{\max} = 1.2$. This approach holds true if all sub-cells show ideal behavior (no low parallel resistance, no low breakthrough voltage) and excluding luminescence coupling effects. J_{SC} values are calculated using a step size of 0.02 in all metric parameters resulting in discrete points in the measurement area.

In a first case, a current matched triple-junction device under the reference spectrum is assumed, where all three sub-cells generate a photocurrent density of 13 mA cm^{-2} (Figure 2a). The point with the highest J_{SC} (current matching point) is, by

definition, at the point $(1, 1, 1)$ corresponding to the reference spectrum. From this point, the current decreases outward in a triangular pattern.

In a second case, a triple-junction solar cell with one strongly limiting sub-cell is considered. This is realized in the calculation by assuming a current density of 6.5 mA cm^{-2} for one sub-cell under the reference spectrum while the remaining two are kept at 13 mA cm^{-2} . Thus, the J_{SC} of the triple-junction solar cell under the reference spectrum at the point $(1, 1, 1)$ is 6.5 mA cm^{-2} . When the top cell is limiting, the current matching point (the origin of the triangular pattern) is shifted toward the corner of the plane of measurement where $A = 3$. For the strong limitation in this example, it is far outside the hexagonal measurement area, within which only vertical lines of the same color are visible (Figure 2b). Similarly, when the current is strongly limited by the middle cell, the current matching point is shifted toward the corner of the measurement plane where $B = 3$ and only horizontal lines of the same color are visible in the measurement area (Figure S1a, Supporting Information). Lastly, if the bottom cell is strongly limiting, the current matching point shifts toward the corner where $C = 3$ and only diagonal lines of the same color parallel to the $B = 3 - A$ line are visible in the measurement plane (Figure S1b, Supporting Information).

In a third case, we consider a current density of 13 mA cm^{-2} for one sub-cell and 6.5 mA cm^{-2} for the other two under the reference spectrum (the J_{SC} of the triple-junction solar cell is 6.5 mA cm^{-2} at the reference spectrum). Again, the values were chosen in a way that the current matching point is outside the measurement area. Inside the area, only one corner of the triangular pattern is visible. Exemplarily this is shown for $j_{\text{top}} = 13 \text{ mA cm}^{-2}$ and $j_{\text{mid}} = j_{\text{bot}} = 6.5 \text{ mA cm}^{-2}$ in Figure 2c. The other scenarios are shown in Figure S1c,d, Supporting Information.

4. Application of Spectrometric Characterization to a Triple-Junction Solar Cell

A spectrometric characterization was applied to a 4 cm^2 GaInP/GaAs/Si triple-junction solar cell using the AM 1.5g

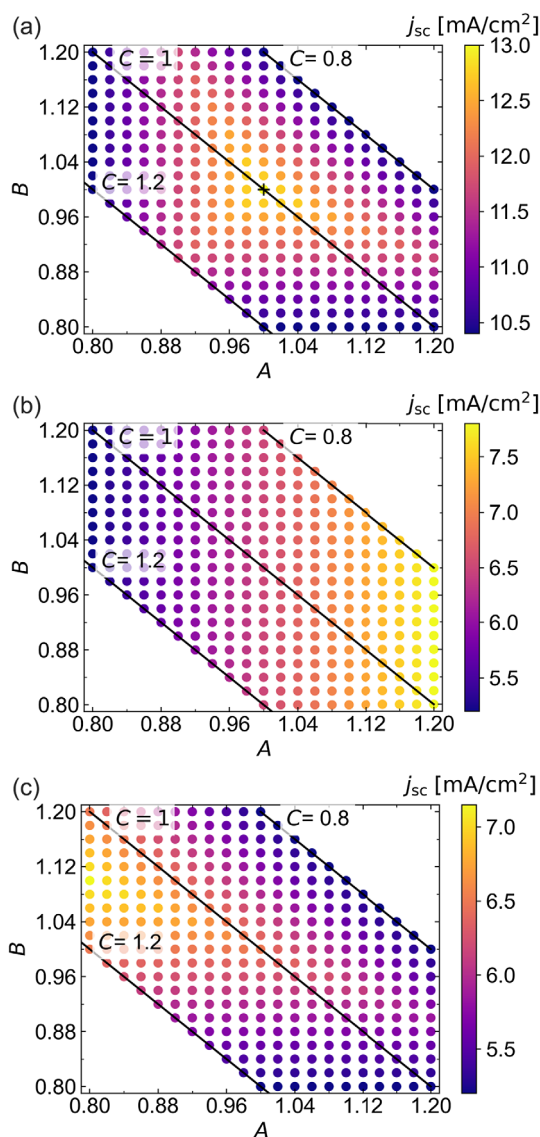


Figure 2. Simulated spectrometric characterization results for different current-matching scenarios. The metric parameters A , B , and C are restricted to $x_{\min} = 0.8$ and $x_{\max} = 1.2$ and the step size is chosen to be 0.02. a) Current-matched device under the reference spectrum ($j_{\text{top}} = j_{\text{mid}} = j_{\text{bot}} = 13 \text{ mA cm}^{-2}$). A triangular pattern around the current-matching point (marked with black +) is visible. b) Strongly limiting top cell ($j_{\text{top}} = 6.5 \text{ mA cm}^{-2}$, $j_{\text{mid}} = j_{\text{bot}} = 13 \text{ mA cm}^{-2}$ under reference spectrum). The current matching point is outside the measurement area. Within the area only vertical lines of the same color are visible. c) Limiting middle and bottom cells ($j_{\text{top}} = 13 \text{ mA cm}^{-2}$, $j_{\text{mid}} = j_{\text{bot}} = 6.5 \text{ mA cm}^{-2}$ under reference spectrum). Again, the current matching point is outside the measurement area where one corner of the triangular pattern is visible.

spectrum as the reference spectrum. The $\text{Ga}_{0.51}\text{In}_{0.49}\text{P}$ top cell, the GaAs middle cell, and the silicon bottom cell have bandgaps of 1.90, 1.43, and 1.12 eV, respectively. The III–V sub-cells were epitaxially grown on each other and connected to the silicon solar cell via wafer bonding. For this work, a solar cell without rear-side light-trapping structure is used. More details can be found in the publication by Cariou et al.^[26]

For the measurement, an LED-based solar simulator (Wavelabs, Sinus 220^[27]) was used. Spectral adjustment was performed using the procedure described by Chojniak et al.^[28] Using this procedure, all spectral settings within the measurement area have been calculated in advance based on the relative spectral responsivities of the three sub-cells. The EQEs are displayed in Figure S2, Supporting Information. Based on the previously determined simulator settings, the full spectrometric characterization was conducted automatically using continuous illumination, without the need for repeated subsequent manual spectral adjustment. A custom software was used to control the light engine of the solar simulator.

For the investigation of the triple-junction solar cell, the metric parameters A , B , and C were restricted to a measurement area defined by $x_{\min} = 0.84$ and $x_{\max} = 1.16$. The measurement area was chosen smaller than the one used for the derivation of the method which is due to intensity limitations of the LED solar simulator. All metric parameters were varied with a step size of 0.02, resulting in 217 spectra for the measurement.

The J_{SC} values obtained from the spectrometric characterization are presented in Figure 3. The maximum J_{SC} is reached for $A^* = 0.96$, $B^* = 0.96$, and $C^* = 1.08$ (black +). This means that the current of the top cell and middle cell needs to be decreased and the current of the bottom cell needs to be increased compared to the AM 1.5 g conditions to reach a current match of all three sub-cells. Thus, at AM 1.5 g conditions ($A = B = C = 1$) the silicon bottom solar cell limits the current of the triple-junction device. The open-circuit voltage is almost independent on the spectral condition (Figure S3a, Supporting Information). As expected, the fill factor shows a minimum at the point where the highest J_{SC} was measured (Figure S3b, Supporting Information), which is the case for high-quality solar cells. Poor-quality solar cells, e.g., with high parallel resistance can show a different behavior.^[18]

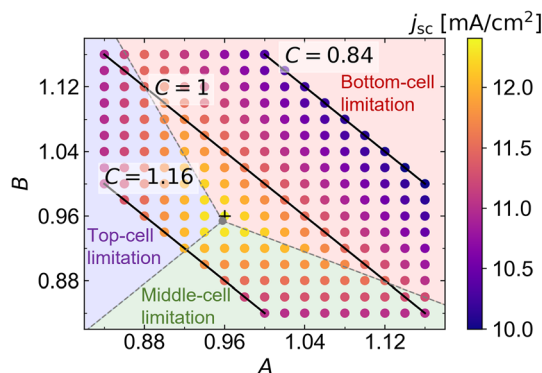


Figure 3. Short-circuit current density (J_{SC}) values obtained from spectrometric characterization of a GaInP/GaAs/Si triple-junction solar cell. The highest J_{SC} (marked with a black +) is obtained under the spectral condition defined by $A^* = 0.96$, $B^* = 0.96$, and $C^* = 1.08$, i.e., the silicon bottom cell is limiting the current at AM 1.5 g conditions. The grey dot represents the fitted current-matching point. The grey-dashed lines from the current matching point toward the corners of the triangular measurement plane divide the plane in three sections. For spectral conditions in the blue-, green-, and red-shaded sections, the top, middle, and bottom cells are current limiting, respectively.

The plane of measurement (Figure 1b) can be divided into three sections by drawing three lines from the current matching point (grey dot in Figure 3) to the corners of the plane of measurement where one of the metric parameters is equal to 3. This representation helps to identify at first view, which sub-cell is limiting the current at a certain spectral condition. In the blue-shaded section of the plane (left part), the top cell is limiting; in the green-shaded section (lower part), the middle cell is limiting; and in the red-shaded section (upper right part), the bottom cell is limiting. Figure S4, Supporting Information, shows these sections in the entire plane of measurement. The current matching point, representing the center of the resulting sections, is calculated in the following.

As the metric parameters were varied in steps of 0.02, the measurement area is divided into discrete measurement points with a limited resolution. The actual current matching point could therefore lie in between several measurement points and does not necessarily have to be identical to the point with the highest measured current. Using a 3D representation in which the measured current is plotted against the parameters A and B , the measured data points can be divided into three areas based on the sub-cell limitation. By applying 2D fits to each set of data points, three planar functions would be defined. The intersection of these functions can be determined as the current matching point.

To facilitate the evaluation of measurements, we propose a simplified method for approximating the current matching point. Therefore, the current matching point is approximated from the mean value of three intersection points of linear fits.

This procedure is similar to the one applied for spectrometric characterization of dual-junction solar cells^[22] but has been extended for triple-junction devices as explained in the following. The application of this routine is described based on the measurement results represented in Figure 3. First, parameter A is fixed to $A = A^* = 0.96$. This corresponds to the vertical line through the point with the highest measured J_{SC} . The J_{SC} values along that line are represented in Figure 4a (note that for a fixed parameter $A = A^*$, B , and C are not independent as for each value of B and C is clearly defined by $C = 3 - A^* - B$ according to Equation (7).) The position of the highest J_{SC} value along this line is determined by the intersection point of two linear fits. This procedure is repeated for a fixed parameter $B = B^* = 0.96$ corresponding to a horizontal line through the point with highest J_{SC} (Figure 4b) and for a fixed parameter $C = C^* = 1.08$ corresponding to a diagonal line through the point with highest J_{SC} (Figure 4c). Metric parameters of the three intersection points are listed in Table S1, Supporting Information. The current matching point is approximated by averaging the non-fixed parameters of the three intersection points and is found for metric parameters $A = 0.958$, $B = 0.954$, and $C = 1.088$. The three intersection points and the resulting current-matching point are represented together with the surrounding measurement points in Figure 4d.

This procedure leads to an approximated current matching point which deviates from the real current matching point by a maximum of 0.005 as determined by the simulation shown in Figure S5, Supporting Information.

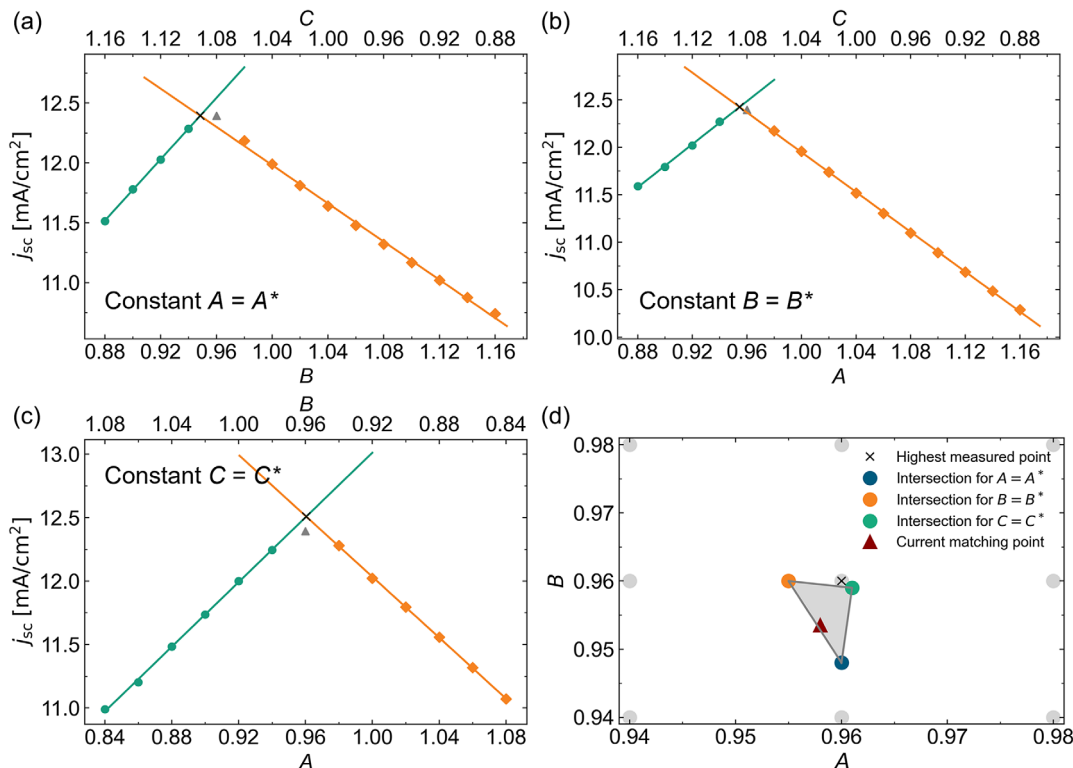


Figure 4. Determination of the current-matching point. J_{SC} values from Figure 3 are plotted along the lines with a) constant A , b) constant B , and c) constant C through the point with the highest measured J_{SC} . d) Intersection points of linear fits and calculated current-matching point in the plane of measurement. Grey dots mark the discrete measurement points, the black \times the position of highest measured J_{SC} .

To check reproducibility the spectrometric characterization was repeated two times on different days. The point with the highest current was the same in all three measurements and the deviations in the calculated current-matching point were <0.006 in all metric parameters (Table S1, Supporting Information). Also, the deviations in J_{SC} were small (maximum 1.8%, but mostly $\approx 0.5\%$) for all metric points (Figure S6, Supporting Information).

Additionally, a measurement was performed with a smaller step size of 0.005 for all metric parameters closely around the current matching point (Figure S7, Supporting Information). This measurement was also repeated a second time. The positions of the maximum J_{SC} of these measurements and the calculated current matching points are in good agreement with the current matching points calculated from the measurements conducted with a lower resolution of metric points (Table S1, Supporting Information). This shows that using a step size of 0.02 for the spectrometric characterization and fitting the current matching point with the routine described earlier leads to reliable results.

5. Relevance of Used Spectral Conditions for Outdoor Performance

In spectrometric characterization, the triple-junction solar cell is measured under different spectral conditions. Under real-field conditions, the solar spectrum is changing permanently depending on the season, the time of the day, and the weather. Following the principle of the previously introduced metric parameters, each outdoor spectrum can be defined by a set of outdoor parameters A' , B' , and C' according to

$$j_{top}^{outdoor} = A' j_{top}^{AM1.5g} \quad (8)$$

$$j_{mid}^{outdoor} = B' j_{mid}^{AM1.5g} \quad (9)$$

$$j_{bot}^{outdoor} = C' j_{bot}^{AM1.5g} \quad (10)$$

Therefore, the sub-cell current densities resulting under a given spectrum $E(\lambda)$ are calculated via

$$j = \int SR(\lambda)E(\lambda)d\lambda \quad (11)$$

The outdoor parameters can be determined if the outdoor spectrum and the spectral responsivities SR of the sub-cells are known. Note that only the relative spectral response is needed for the determination of A' , B' , and C' , as it appears on both sides of Equation (8)–(10).^[18]

The outdoor spectra are not necessarily lying on the plane of measurement as defined earlier and as shown in Figure 1, as $A' + B' + C' \neq 3$ in general. However, they can be projected on the plane of measurement using

$$\begin{pmatrix} A \\ B \\ C \end{pmatrix} = \frac{3}{A' + B' + C'} \begin{pmatrix} A' \\ B' \\ C' \end{pmatrix} \quad (12)$$

which maintains the current ratios between the sub-cells. Thus, we check whether the sub-cell current balancing investigated

within the spectrometric characterization also occurs in outdoor applications of the multi-junction solar cell.

As an example, global outdoor spectra from one clear-sky day (18.05.2022) in Freiburg/Germany (48.01°N, 7.83°E), measured every 15 min using a spectroradiometer, were analyzed. Outdoor parameters A' , B' , and C' were determined using the spectral responsivities of the GaInP/GaAs//Si triple-junction solar cell utilized for the spectrometric measurement and projected to the plane of measurement by Equation (12) (Figure 5). Each circle plotted in the graph corresponds to one spectrum, while the color of the circle is connected to the corresponding global irradiance. Most of the spectra are lying within the measurement area (1 ± 0.16). Only a few spectra are outside. However, these are spectra measured in the early morning and late evening which have a comparable low overall irradiance and thus do not significantly contribute to the power generation of the solar cell throughout the day. This shows that the spectral conditions used for spectrometric characterization not only allow for determination of the current matching situation but also have a relevance for outdoor applications and can therefore serve as input for energy yield analysis.

During the course of the day, the global irradiance increases until around 12:30 p.m. and afterward decreases again. Also, a clear shift in the spectrum, mainly affecting parameter A , is visible in parallel. There are three main parameters affecting the outdoor spectral conditions: AM, aerosol optical depth, and precipitable water.^[29] Throughout the day, AM changes significantly based on the position of the sun. Since changes in AM mainly affect the short-wavelength range of the solar spectrum, increasing AM leads to less high energy photons reaching the solar cell.^[29] Thus, variations in AM are primarily visible in the current of the top cell and therefore parameter A . In contrast aerosol optical depth, mainly affecting parameters A and B , and

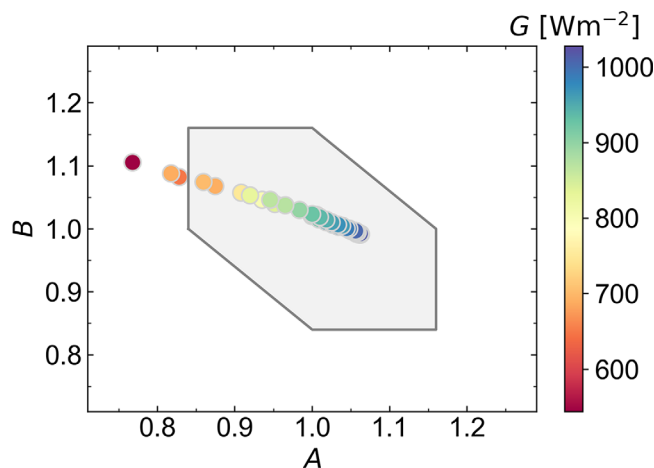


Figure 5. Metric parameters for the GaInP/GaAs//Si triple-junction solar cell obtained from global outdoor spectra measured during 1 day (18.05.2022) in Freiburg/Germany (48.01°N, 7.83°E) projected on the plane of measurement. The marked grey area corresponds to the measurement area used for the spectrometric characterization in this work. Almost all outdoor conditions during the investigated day are covered by the measurement area (1 ± 0.16). The color of the circles indicates the global irradiance G .

the amount of precipitable water, mainly affecting parameters B and C , did not change significantly throughout the investigated day. Accordingly, variations in B and C are small compared to A .

6. Summary and Conclusion

In this work, the method of spectrometric characterization described in detail for dual-junction solar cells by Meusel et al.^[18] has been extended and applied to triple-junction solar cells. As a key aspect of the introduced approach, it was explained how clearly defined measurement conditions are derived which all lie on a plane of measurement. This results in consistent measurement conditions allowing for characterization and comparison of different triple-junction solar cells. A spectrometric measurement has been conducted for a III–V on Si triple-junction solar cell using an LED-based solar simulator. The spectral conditions utilized for the measurement were calculated in advance and automatically adjusted. As it is not feasible to cover the whole plane of measurement, an area of measurement around the AM 1.5 g spectrum was defined. To accurately determine the current matching point from the discrete measurement points in the plane, a fit routine has been proposed. The result of this fitting procedure has been compared to a measurement with high resolution around the current matching point. A good agreement between both values has been shown, proving the applicability of the introduced fitting approach. Finally, it has been exemplarily shown that the spectra within the measurement area also represent relevant outdoor conditions, which underlines the relevance of the presented characterization procedure exceeding the mere determination of a multi-junction cell's current matching condition.

The measurement was described for a III–V on Si triple-junction solar cell under the AM 1.5 g spectrum. However, it is not limited to this case. Other reference spectra and other types of solar cells could be used. Especially for perovskite-based triple-junction solar cells this method could be beneficial as integrating measured EQEs can lead to strong misinterpretations of the current-matching situation due to dynamic effects. However, a certain stability of the devices is required as a high number of IV sweeps (in this example: 217) have to be conducted.

In this work, the principle of the method was derived and a stable solar cell with nearly ideal IV properties was chosen for a proof of concept. If subcells with nonideal IV curves (low parallel resistance or low reverse breakdown voltage) are involved, the evaluation gets more complex as not the triple-junction J_{SC} , but rather the J_{SC} of the subcells should be considered for determining the current-matching point. Nevertheless, the method presented in this work provides new possibilities for the detailed characterization of all types of multi-junction solar cells, enabling valuable insights to the characteristics and interaction of the sub-cells involved.

Supporting Information

Supporting Information is available from the Wiley Online Library or from the author.

Acknowledgements

This work was supported by the German Federal Ministry for Economic Affairs and Climate Action (BMWK) under contract number 03EE1132A (RIESEN) and partially supported by the European Union through the Horizon Europe project TRIUMPH under the contract number 101075725. Open Access funding enabled and organized by Projekt DEAL.

Conflict of Interest

The authors declare no conflict of interest.

Data Availability Statement

The data that support the findings of this study are available from the corresponding author upon reasonable request.

Keywords

current mismatches, multi-junction solar cells, photovoltaics, spectrometric characterizations, triple-junction solar cells

Received: September 29, 2023

Revised: November 20, 2023

Published online: December 12, 2023

- [1] T. Niewelt, B. Steinhäuser, A. Richter, B. Veith-Wolf, A. Fell, B. Hammann, N. E. Grant, L. Black, J. Tan, A. Youssef, J. D. Murphy, J. Schmidt, M. C. Schubert, S. W. Glunz, *Sol. Energy Mater. Sol. Cells* **2022**, 235, 111467.
- [2] KAUST Claims 33.7% Efficiency for Perovskite/Silicon Tandem Solar Cell, <https://www.pv-magazine.com/2023/05/30/kaust-claims-33-7-efficiency-for-perovskite-silicon-tandem-solar-cell/> (accessed: September 2023).
- [3] M. Yamaguchi, *Sol. Energy Mater. Sol. Cells* **2003**, 75, 261.
- [4] J. Werner, F. Sahli, F. Fu, J. J. Diaz Leon, A. Walter, B. A. Kamino, B. Niesen, S. Nicolay, Q. Jeangros, C. Ballif, *ACS Energy Lett.* **2018**, 3, 2052.
- [5] J. Zheng, G. Wang, W. Duan, M. A. Mahmud, H. Yi, C. Xu, A. Lambert, S. Bremner, K. Ding, S. Huang, A. W. Y. Ho-Baillie, *ACS Energy Lett.* **2022**, 7, 3003.
- [6] Y. J. Choi, S. Y. Lim, J. H. Park, S. G. Ji, J. Y. Kim, *ACS Energy Lett.* **2023**, 8, 3141.
- [7] M. Heydarian, M. Heydarian, A. J. Bett, M. Bivour, F. Schindler, M. Hermle, M. C. Schubert, P. S. C. Schulze, J. Borchert, S. W. Glunz, *ACS Energy Lett.* **2023**, 8, 4186.
- [8] P. Schygulla, R. Müller, D. Lackner, O. Höhn, H. Hauser, B. Bläsi, F. Predan, J. Benick, M. Hermle, S. W. Glunz, F. Dimroth, *Prog. Photovoltaics* **2022**, 30, 869.
- [9] J. Metzendorf, *Appl. Opt.* **1987**, 26, 1701.
- [10] M. Meusel, C. Baur, G. Létay, A. W. Bett, W. Warta, E. Fernandez, *Prog. Photovoltaics* **2003**, 11, 499.
- [11] M. A. Steiner, J. F. Geisz, T. E. Moriarty, R. M. France, W. E. McMahon, J. M. Olson, S. R. Kurtz, D. J. Friedman, *IEEE J. Photovoltaics* **2013**, 3, 879.
- [12] M. Saliba, L. Etgar, *ACS Energy Lett.* **2020**, 5, 2886.
- [13] M. Mundus, B. Venkataramanachar, R. Gehlhaar, M. Kohlstädt, B. Niesen, W. Qiu, J. P. Herterich, F. Sahli, M. Bräuninger, J. Werner, J. Hohl-Ebinger, G. Uytterhoeven, U. Würfel, C. Ballif,

- M. C. Schubert, W. Warta, S. W. Glunz, *Sol. Energy Mater. Sol. Cells* **2017**, *172*, 66.
- [14] L. V. Mercaldo, E. Bobeico, A. de Maria, M. Della Noce, M. Ferrara, L. Lancellotti, A. Romano, G. V. Sannino, G. Nasti, A. Abate, P. Delli Veneri, *Energy Technol.* **2022**, *10*, 2200748.
- [15] Y. Hishikawa, H. Shimura, T. Ueda, A. Sasaki, Y. Ishii, *Curr. Appl Phys.* **2016**, *16*, 898.
- [16] T. Song, C. Mack, R. Williams, D. J. Friedman, N. Kopidakis, *Sol. RRL* **2022**, *6*, 2200800.
- [17] R. Adelhelm, K. Bücher, *Sol. Energy Mater. Sol. Cells* **1998**, *50*, 185.
- [18] M. Meusel, R. Adelhelm, F. Dimroth, A. W. Bett, W. Warta, *Prog. Photovoltaics* **2002**, *10*, 243.
- [19] M. Meusel, C. Baur, G. Siefert, F. Dimroth, A. W. Bett, W. Warta, *Sol. Energy Mater. Sol. Cells* **2006**, *90*, 3268.
- [20] E. F. Fernandez, A. J. G. Loureiro, P. J. P. Higuera, G. Siefert, in *Proc. of the 8th Spanish Conf. on Electron Devices, CDE'2011*, IEEE, Palma de Mallorca, Spain **2011**, pp. 1–4, <https://doi.org/10.1109/sced.2011.5744222>.
- [21] G. Siefert, C. Baur, M. Meusel, F. Dimroth, A. W. Bett, W. Warta, in *Conf. Record of the Twenty-Ninth IEEE Photovoltaic Specialists Conf. 2002*, IEEE, Piscataway, NJ **2002**, pp. 836–839 <https://doi.org/10.1109/pvsc.2002.1190709>.
- [22] A. J. Bett, D. Chojniak, M. Schachtner, S. K. Reichmuth, Ö. Ş. Kabaklı, P. S. C. Schulze, O. Fischer, F. Schindler, J. Hohl-Ebinger, G. Siefert, M. C. Schubert, *Sol. RRL* **2023**, *7*, 2200948.
- [23] M. Heydarian, C. Messmer, A. J. Bett, M. Heydarian, D. Chojniak, Ö. Ş. Kabaklı, L. Tutsch, M. Bivour, G. Siefert, M. C. Schubert, J. C. Goldschmidt, M. Hermle, S. W. Glunz, P. S. C. Schulze, *Sol. RRL* **2023**, *7*, 2200930.
- [24] Ö. Ş. Kabaklı, J. Kox, L. Tutsch, M. Heydarian, A. J. Bett, S. Lange, O. Fischer, C. Hagendorf, M. Bivour, M. Hermle, P. S. Schulze, J. C. Goldschmidt, *Sol. Energy Mater. Sol. Cells* **2023**, *254*, 112246.
- [25] A. J. Bett, P. S. C. Schulze, K. M. Winkler, Ö. S. Kabaklı, I. Ketterer, L. E. Mundt, S. K. Reichmuth, G. Siefert, L. Cojocar, L. Tutsch, M. Bivour, M. Hermle, S. W. Glunz, J. C. Goldschmidt, *Prog. Photovoltaics* **2019**, *28*, 99.
- [26] R. Cariou, J. Benick, F. Feldmann, O. Höhn, H. Hauser, P. Beutel, N. Razek, M. Wimplinger, B. Bläsi, D. Lackner, M. Hermle, G. Siefert, S. W. Glunz, A. W. Bett, F. Dimroth, *Nat. Energy* **2018**, *3*, 326.
- [27] M. L. D. Scherff, J. Nutter, P. Fuss-Kailuweit, J. Suthues, T. Brammer, *Jpn. J. Appl. Phys., Part 1* **2017**, *56*, 08MB24.
- [28] D. Chojniak, A. J. Bett, J. Hohl-Ebinger, S. K. Reichmuth, M. Schachtner, G. Siefert, in *SiliconPV 2022, the 12th Int. Conf. on Crystalline Silicon Photovoltaics*, AIP Publishing, Konstanz, Germany **2023**, p. 30003, <https://doi.org/10.1063/5.0140990>.
- [29] C. Stark, M. Theristis, in *2015 IEEE 42nd Photovoltaic Specialist Conf. (PVSC)*, IEEE, Piscataway, NJ **2015**, pp 1–5, <https://doi.org/10.1109/pvsc.2015.7355836>